Journal of Power Sources 236 (2013) 54–60

Contents lists available at SciVerse ScienceDirect

Journal of Power Sources

journal homepage: www.elsevier.com/locate/jpowsour

Short communication

In-situ controllable synthesis and performance investigation of carbon-coated monoclinic and hexagonal $LiMnBO_3$ composites as cathode materials in lithium-ion batteries

Shouli Li, Liqiang Xu*, Guangda Li, Meng Wang, Yanjun Zhai

Key Laboratory of the Colloid and Interface Chemistry (Shandong University), Ministry of Education, and School of Chemistry and Chemical Engineering, Shandong University, Jinan 250100, PR China

HIGHLIGHTS

- The m-$LiMnBO_3$/C and h-$LiMnBO_3$/C composites have been selectively and conveniently prepared.
- The long cycle stability of h-$LiMnBO_3$/C is firstly reported in this study.
- It is the first time to report the rate performance of m-$LiMnBO_3$/C composite.

GRAPHICAL ABSTRACT

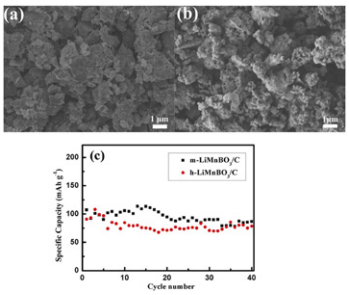

ARTICLE INFO

Article history:
Received 13 November 2012
Received in revised form
10 February 2013
Accepted 12 February 2013
Available online 20 February 2013

Keywords:
Composite materials
Phase control
Borates
Lithium-ion battery

ABSTRACT

The phase controllable synthesis of carbon-coated monoclinic $LiMnBO_3$ (m-$LiMnBO_3$/C) and hexagonal $LiMnBO_3$ (h-$LiMnBO_3$/C) composites has been achieved via an in-situ carbothermal solid state synthesis approach only through the modulation of the reaction temperature. The h-$LiMnBO_3$/C particles keep high cycle stability and retain 86.5% of the initial discharge capacity (90.7 mAh g^{-1}) after 40 cycles at 0.05 C (11 mA g^{-1}) within 1.25–4.80 V, while the m-$LiMnBO_3$/C composites display a first discharge capacity of 107 mAh g^{-1} and a capacity retention rate of 80.8% after 40 cycles. The rate performance of m-$LiMnBO_3$/C has been tested for the first time, which has a capacity of 74.4 mAh g^{-1} at the discharge rate of 0.1 C (22 mA g^{-1}). The enhanced electrochemical performance might be largely attributed to the uniformly coated carbon layers and the reduced particle size of the as-obtained products. The electrochemical impedance spectroscopy (EIS) analysis reveals that the smaller charge transfer resistance (R_{ct}) and higher electronic conductivity of the $LiMnBO_3$/C composites were obtained at 55 °C than those at 25 °C. The as-obtained $LiMnBO_3$/C composites with controllable phases and high performances enable their promising applications as cathode materials for lithium-ion rechargeable batteries.

© 2013 Elsevier B.V. All rights reserved.

1. Introduction

Borates ($LiMBO_3$, M = Fe, Mn) are kinds of attractive cathode materials for lithium-ion rechargeable battery owing to their relatively high theoretical capacity (~220 mAh g^{-1}) and little volume changes [1]. They also exhibit relatively high stable structure and adjustable voltage platform characteristics [2]. Since the first report that Li could be reinserted reversibly from the $LiMBO_3$ (M = Co, Fe, Mn) materials in 2001 [3], increasing efforts have been made to improve the electrochemical performances of these materials during the past decade through many new approaches such as carbon addition, nanocrystallization, and ion doping etc. [4–6].

* Corresponding author. Tel.: +86 531 88364543; fax: +86 531 88366280.
E-mail address: xulq@sdu.edu.cn (L. Xu).

0378-7753/$ – see front matter © 2013 Elsevier B.V. All rights reserved.
http://dx.doi.org/10.1016/j.jpowsour.2013.02.027

Among these methods, carbon coating is one of the most effective approaches for reducing the structure instability and capacity degradation of individual $LiMBO_3$ materials when encounter with moist air and electrolyte, and for elevating the capacity and cycle stability of the target borate materials. For instance, $LiFeBO_3$/C obtained through a solid state reaction using Li_2CO_3, $FeC_2O_4{\cdot}2H_2O$, B_2O_3, ketchen black and vapour grown carbon fibre as raw materials in Ar atmosphere at 873 K had a discharge capacity of 190 mAh g^{-1} at 0.05 C in the voltage range of 1.5–4.5 V under charging mode at constant voltage of 4.5 V until the current decayed down to 1 mA g^{-1} [7]; Under constant current charge–discharge mode, the initial discharge capacity of $LiFeBO_3$ was improved from 125.8 to 158.3 mAh g^{-1} at 5 mA g^{-1} within a voltage window of 1.0–4.8 V after carbon coating [8].

$LiMnBO_3$ (which has two polymorphs: hexagonal and monoclinic phases) has higher theoretical energy density and average voltage (4.1 V/3.7 V) than those of $LiFeBO_3$ (monoclinic phase) although their theoretical capacities have little difference [9]. The m-$LiMnBO_3$ material was initially synthesized below 400 °C through the hydrothermal process in 1978 [10], but its electrochemical property was not reported until 2011, with a second cycle discharge capacity of about 100 mAh g^{-1} at 0.05 C within 2.0–4.5 V under constant current and constant voltage mode [11]. The bare h-$LiMnBO_3$ material was announced to have a discharge capacity of 75.5 mAh g^{-1} at the current density of 5 mA g^{-1} within a window of 1.0–4.8 V in 2010 [2]. Recently, nanoscaled h-$LiMnBO_3$ particles were firstly obtained via a sol–gel method, which presented a first discharge capacity of 136 mAh g^{-1} in the voltage range of 1.7–4.7 V at 11 mA g^{-1} [5]. Up to date, the $LiMBO_3$ materials were mainly fabricated through solid state process at 500–850 °C for 12–15 h under inert atmosphere [2,12], while the two-step calcination processes were usually required together with the intermediate ball-milling process to minimize the particle size after the first calcination process. The carbon-coated h-$LiMnBO_3$was usually fabricated via the calcination of the mixture of h-$LiMnBO_3$ and carbon sources under inert atmosphere [11]. To further facilitate the fabrication process and improve the carbon coating efficiency, new developments and strategies are required for these materials. In this study, $LiMnBO_3$/C composites with tunable phases have been obtained through in-situ carbothermal solid state synthesis approach under relatively low temperature. For example, the h-$LiMnBO_3$/C particles were obtained at 750 °C. These particles keep high cycle stability and retain 86.5% of the initial discharge capacity (90.7 mAh g^{-1}) after 40 cycles at 11 mA g^{-1} within 1.25–4.80 V under constant current charge-discharge mode. The actual discharge capacity of h-$LiMnBO_3$ is obviously enhanced via in-situ carbon coating process compared with that of the previous report [2]. While the m-$LiMnBO_3$/C particles could be obtained at 500–600 °C. The m-$LiMnBO_3$/C particles prepared at 600 °C have an initial discharge capacity of up to 107 mAh g^{-1}. It is notable that even if the current density is increased to 22 mA g^{-1}, the specific discharge capacity of 74.4 mAh g^{-1} still can be obtained. The above results indicate that the $LiMnBO_3$/C materials with controllable phases obtained via the convenient in-situ carbothermal solid state synthesis method are promising cathode materials for lithium-ion rechargeable batteries.

2. Experimental

2.1. Sample preparation

All the raw materials used here were of analytic grade without further purification. h-$LiMnBO_3$/C and m-$LiMnBO_3$/C powders were controllable prepared via adjusting the heating temperature through in-situ carbothermal solid state synthesis with the stage-temperature-programmed calcination process [11,13]. In a typical process,10 mmol $LiOH{\cdot}H_2O$, 10 mmol $MnCO_3$, 10 mmol H_3BO_3 and 2.5 mmol ascorbic acid were dispersed into ethanol and ball-milled for 5 h, then the solvents were evaporated in the vacuum oven at 60 °C. For the preparation of h-$LiMnBO_3$/C, the precursor was calcined at 250 °C for 3 h at first, and then at 750 °C for 10 h with a increasing heating rate of 5 °C per minute under Ar atmosphere in a tube furnace. For the synthesis of m-$LiMnBO_3$/C, the precursor was calcined at 250 °C for 3 h and then at 500–600 °C for 10 h.

2.2. Characterization

The X-ray diffraction (XRD) patterns were measured on a Bruker D8 advanced X-ray diffractometer equipped with graphite-monochromatized CuKα radiation (λ = 1.5418 Å). The Raman spectrum was recorded at ambient temperature on a LABRAM-HR confocal laser MicroRaman spectrometer with an argon-ion laser at an excitation wavelength of 514.5 nm. The transmission electron microscopy (TEM, JEM-2011), field emission scanning electron microscope (FESEM; JEOL JSM-6700F) and high-resolution TEM (HRTEM, JEM-2100, 200 kV) were used to characterize the morphology and size of the samples.

2.3. Electrochemical measurements

The electrochemical discharge-charge performances of the samples were tested on a Land battery test system (CT2001A) at 25 °C. The working electrodes were consisted of 70 wt% active materials (h-$LiMnBO_3$/C or m-$LiMnBO_3$/C), 20 wt% carbon black, and 10 wt% poly(vinylidene fluoride) (PVDF). n-Methylpyrrolidone (NMP) was used as the solvent. The mixed slurry with thickness of 200 μm was coated onto a piece of Al foil and dried in vacuum oven at 80 °C for 12 h, then cut into discs with diameter of 12 mm. The weight of electrode pieces was in the range of 2–3 mg except that of the pristine Al foil. And the mass calculation of the active $LiMnBO_3$/C materials was carried out based on 70% of the mass of electrode piece. Nickel foams were used as the current collector, and Celgard 2300 microporous polypropylene membrane was used as the separator. The electrolyte was composed of 1 mol $L^{-1}LiPF_6$ dissolved ethylene carbonate/dimethyl carbonate/diethyl carbonate (EC/DMC/DEC, volume ratio was 1:1:1). Lithium foils with the diameter of 15 mm and the thickness of 0.4 mm were used as the counter electrodes. The button batteries were assembled in an argon-filled glove box and cycled at different charge-discharge current densities (5, 11, 22 mA g^{-1}) within voltage limit of 1.25–4.80 V. The electrochemical impedance spectroscopy (EIS) was measured with a Princeton Applied Research by applying an alternating current voltage of 10 mV in the frequency from 10 mHz to 100 kHz at open-circuit voltage ($\sim$3 V) before charge-discharge test.

3. Results and discussion

3.1. Structure and morphology characterizations

The typical XRD patterns of the as-obtained $LiMnBO_3$/C samples are shown in Fig. 1a–b. All the diffraction peaks can be assigned to highly crystalline m-$LiMnBO_3$/C and h-$LiMnBO_3$/C without any detectable impurities. The typical XRD pattern of pure m-$LiMnBO_3$/C shown in Fig. 1a is consistent with that mentioned in the reference (JCPDS card no. 83-2342, space group: C2/c) [10,11]. Fig. 1b shows the XRD pattern of h-$LiMnBO_3$/C (JCPDS no. 53-0371, space group: P-6). No obvious peaks of graphite can be observed from the above pattern owing to their low loading amount or low crystallinity [14]. Raman spectra analyses were carried out to further

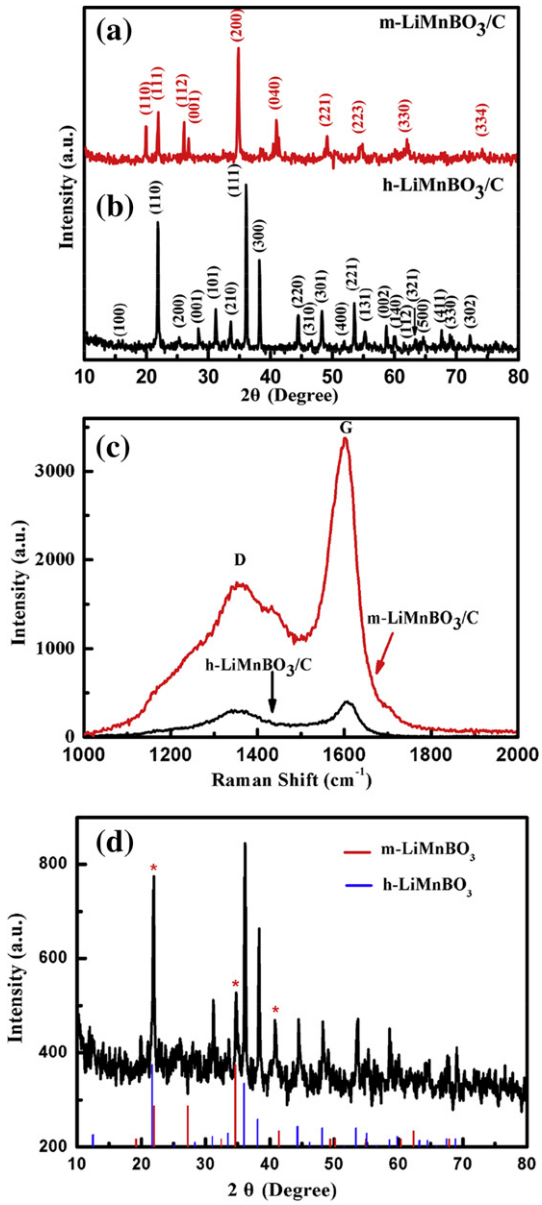

Fig. 1. (a, b) XRD patterns of the as-obtained m-$LiMnBO_3$/C and h-$LiMnBO_3$/C powders; (c) Raman spectra of the m-$LiMnBO_3$/C and h-$LiMnBO_3$/C powders; (d) The XRD pattern of final product prepared at 650 °C.

detect the existence of graphite coated on the surfaces of m-$LiMnBO_3$/C and h-$LiMnBO_3$/C. It is observed from Fig. 1c that there are two peaks with strong intensity centred at ~1365 cm^{-1} (D-band) and 1600 cm^{-1}(G-band). The former corresponds to the vibrations of carbon atoms with dangling bonds in planar terminations of disordered graphite, while the latter correlates to the vibration in all sp^2-band carbon atoms in a two-dimensional hexagonal lattice [15,16]. These results evidenced that graphite existed in both of the samples. The intensity ratios of D-band and G-band (I_D/I_G) are generally used to evaluate the disorder degrees in graphite layers. The higher of the I_D/I_G ratios, the more defects are existed in graphite layers [17,18]. In this experiment, the I_D/I_G values calculated from the Raman spectra of m-$LiMnBO_3$/C and h-$LiMnBO_3$/C are 0.51 and 0.74, respectively, indicating the higher graphitization degree or less defect of graphite in m-$LiMnBO_3$/C than that of in h-$LiMnBO_3$/C. The high graphitization degree is beneficial to enhance the electronic conductivity of the target cathode materials [19,20].

A series of contrast experiments were carried out through adjusting the reaction parameters on the controllable preparation of m-$LiMnBO_3$/C and h-$LiMnBO_3$/C. In the Table 1, the symbol "—" means "without" and the symbol of 'Temperature (°C)/Time (h)' means the reaction is consisted of two stage-temperature-programmed calcination processes, the under part displays reaction time and the upper part presents reaction temperature. The as-prepared $LiMnBO_3$/C marked with asterisk was used for the following analysis. It can be seen that if keeping other conditions unchanged, Li_2CO_3 and $LiOH\cdot H_2O$ are good alternative lithium sources for the preparation of m-$LiMnBO_3$/C and h-$LiMnBO_3$/C. Beside them, $LiBO_2$could also act as lithium source in this process, and meanwhile it served as a boron source. Ascorbic acid was used for the achievement of uniform carbon coating on the surfaces of $LiMnBO_3$ owing to its appropriate reducing ability. The phase controllable preparation of $LiMnBO_3$/C was achieved by controlling the heating temperature. The whole reaction process was in-situ carbothermal synthesis with the stage-temperature-programmed calcination process in the absence of traditionally required intermediate ball milling process. The aim of the former calcination process in 200–300 °C was for the partially decomposition of the reactants, while the subsequent latter calcination process was used for the formation of target products with controllable phases and with high crystallinity.

The results in Table 1 indicate that m-$LiMnBO_3$/C could be obtained in 500–600 °C for 10–15 h, and h-$LiMnBO_3$/C could be fabricated at 750 °C. When the temperature was set at 650 °C, m-$LiMnBO_3$/C and h-$LiMnBO_3$/C were co-existed in the final products (see Fig. 1d, in which the peaks marked with asterisk belong to m-$LiMnBO_3$). We believe that the absence of traditional and required intermediate ball-milling process, the simplified operation, the reduced energy consumption together with the use of green solvent (ethanol was used instead of acetone etc.) make it a highly promising way for the scaled up fabrication of $LiMnBO_3$/C with controllable phases.

The SEM images of $LiMnBO_3$ and $LiMnBO_3$/C are shown in the Fig. 2. The size of h-$LiMnBO_3$/C composites is about 1–2 μm (Fig. 2b), which is smaller than that of bare h-$LiMnBO_3$ particles (2–3 μm, in Fig. 2a). The m-$LiMnBO_3$ lumps with the size of ~2 μm are composed of smaller nanoscaled particles (Fig. 2c). After carbon coating, the size of m-$LiMnBO_3$/C particles (Fig. 2d) reduces to about 1 μm with the carbon layer of 2–5 nm (see Fig. S1 in the Supplementary information) and the lumps are still composed of nanoscaled particles with size of less than 200 nm. Therefore, in-situ carbon coating not only could reduce the size of target product, but also could be expected to improve the electrochemical performance of the final product.

The TEM images of individual h-$LiMnBO_3$ and m-$LiMnBO_3$ are displayed in Fig. 3a and Fig. 3d (the particles are agglomerated to some extent), while those of h-$LiMnBO_3$/C and m-$LiMnBO_3$/C are shown in Fig. 3b and Fig. 3e (with relative better dispersity and smaller sizes), respectively. It is clear that the thin carbon layers (with light grey colour) were coated on the edges of dark $LiMnBO_3$ particles (Fig. 3e). The result of the HRTEM image of h-$LiMnBO_3$/C powders (Fig. 3c) shows that the interior planar distance between the adjacent lattice fringes is 0.36 nm, which corresponds to the d-spacing value of the (200) plane of h-$LiMnBO_3$. The clear resolved lattice fringes with d-spacing values of 0.26 and 0.33 nm shown in Fig. 3f are consonant with (200) and (112) plane values of the m-$LiMnBO_3$, while the outer irregular shaped lattice fringes are associated with the graphite with low crystallinity. These results further confirm the formation of m-$LiMnBO_3$/C and h-$LiMnBO_3$/C composites.

Table 1
The detailed preparation conditions of $LiMnBO_3$ and $LiMnBO_3$/C.

Li source	B source	Mn source	Carbon source	Temperature (°C)/Time (h)	Product
$LiOH·H_2O$	H_3BO_3	$MnCO_3$	–	$\frac{250}{3}\rightarrow\frac{750}{10}$	h-$LiMnBO_3$
			–	$\frac{250}{3}\rightarrow\frac{750}{10}$	h-$LiMnBO_3$
			–	$\frac{250}{3}\rightarrow\frac{500}{10}$	m-$LiMnBO_3$
			Ascorbic acid	$\frac{250}{3}\rightarrow\frac{750}{10}$	h-$LiMnBO_3$/C*
			Ascorbic acid	$\frac{250}{3}\rightarrow\frac{500}{10}$	m-$LiMnBO_3$/C
			Ascorbic acid	$\frac{250}{3}\rightarrow\frac{600}{10}$	m-$LiMnBO_3$/C*
Li_2CO_3	H_3BO_3	$MnCO_3$	–	$\frac{250}{3}\rightarrow\frac{750}{15}$	h-$LiMnBO_3$
			–	$\frac{250}{3}\rightarrow\frac{500}{10}$	m-$LiMnBO_3$
			Ascorbic acid	$\frac{250}{3}\rightarrow\frac{750}{15}$	h-$LiMnBO_3$/C
			Ascorbic acid	$\frac{250}{3}\rightarrow\frac{500}{10}$	m-$LiMnBO_3$/C
$LiBO_2$	–	$MnCO_3$	–	$\frac{250}{3}\rightarrow\frac{750}{15}$	h-$LiMnBO_3$
			–	$\frac{250}{3}\rightarrow\frac{500}{10}$	m-$LiMnBO_3$
			Ascorbic acid	$\frac{250}{3}\rightarrow\frac{750}{15}$	h-$LiMnBO_3$/C
			Ascorbic acid	$\frac{250}{3}\rightarrow\frac{500}{10}$	m-$LiMnBO_3$/C

3.2. Electrochemical characterization

Fig. 4 show the 1st, 2nd and 40th cycle charge–discharge curves of m-$LiMnBO_3$/C and h-$LiMnBO_3$/C electrodes in the voltage range of 1.25–4.80 V vs. Li/Li^+(the related voltage vs. energy density curves are displayed in Fig. S2). The irreversible capacity loss may be ascribed to the formation of solid electrolyte interphase (SEI) film or the decomposition of electrolyte under the high voltage (>4.5 V) etc. [21–23]. The similar phenomenon has also been observed on Li_2MnSiO_4 [24]. It is obvious that these $LiMnBO_3$materials have no obvious wide voltage platforms, which corresponds to the results of previous report [11]. When the voltage was set in the range of 3.0–4.8 V, both m-$LiMnBO_3$/C and h-$LiMnBO_3$/C achieved capacities are less than 30% of the total discharge capacity, which might be ascribed to the possible charge-discharge mechanism (see Fig. S3), and this phenomena is similar to that of $LiFeBO_3$ [5,25]. However, the exact mechanisms of the as-obtained $LiMnBO_3$/C materials should still be further investigated.

Fig. 5a displays the cycle stability curves of m-$LiMnBO_3$/C and h-$LiMnBO_3$/C within window of 1.25–4.80 V at the current density of

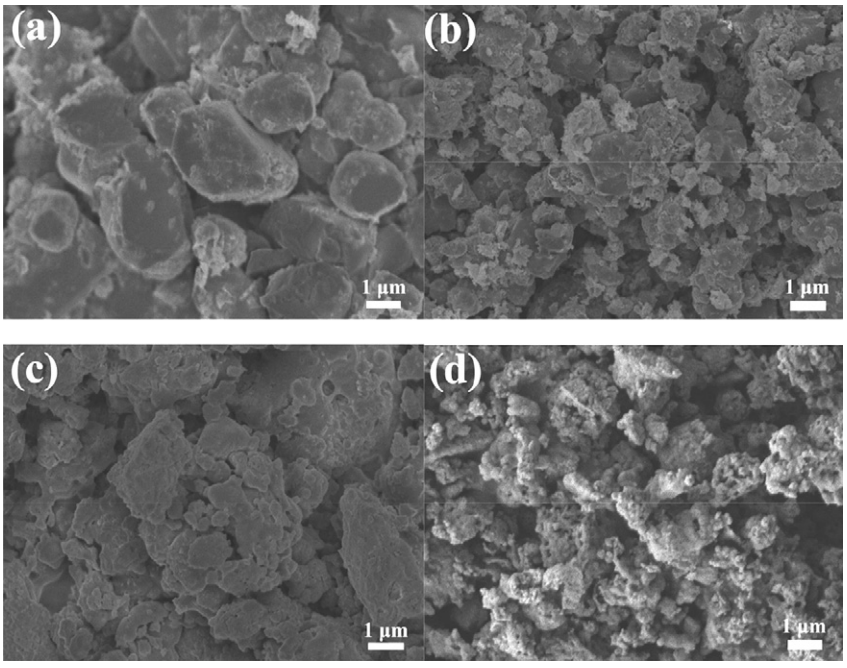

Fig. 2. SEM images of the samples: (a) h-$LiMnBO_3$, (b) h-$LiMnBO_3$/C, (c) m-$LiMnBO_3$, (d) m-$LiMnBO_3$/C.

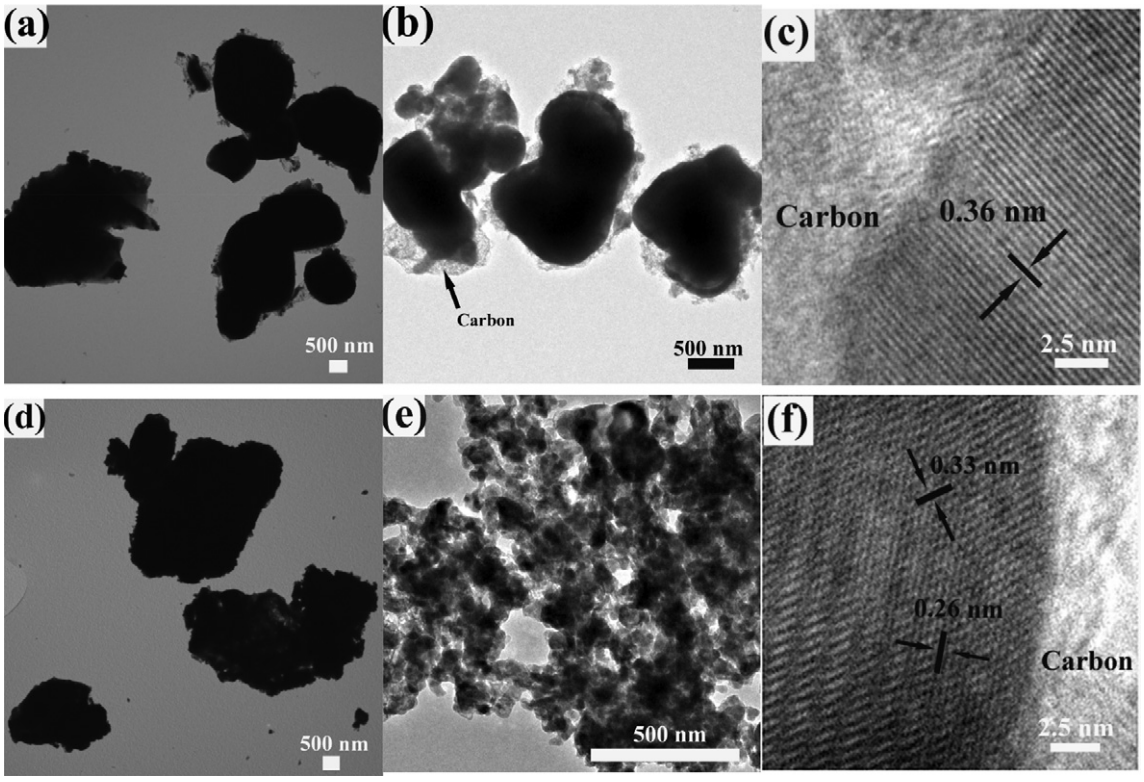

Fig. 3. TEM images of the samples: (a) h-$LiMnBO_3$, (b) h-$LiMnBO_3$/C, (d) m-$LiMnBO_3$, (e) m-$LiMnBO_3$/C; HRTEM images: (c) h-$LiMnBO_3$/C and (f) m-$LiMnBO_3$/C.

11 mA g^{-1}. The first discharge capacity of m-$LiMnBO_3$/C is 107 mAh g^{-1}, and maintains at 86.7 mAh g^{-1} after 40 cycles. For the h-$LiMnBO_3$/C material, an initial discharge capacity of 90.7 mAh g^{-1} is obtained, and 86.5% of the capacity can be remained after 40 cycles, indicating a high reversibility of the materials. When the voltage window was narrowed to 2.0–4.5 V, both m-$LiMnBO_3$/C and h-$LiMnBO_3$/C can still display good performances (see Fig. S4 and Fig. S5). The smaller particle size and more uniform carbon coating of the as-obtained m-$LiMnBO_3$/C (with size of ~200 nm) than that of h-$LiMnBO_3$/C (with particle size of ~1–2 μm) might be the important factors that lead to the superior performances of m-$LiMnBO_3$/C than h-$LiMnBO_3$/C. Because small particle size can reduce the lithium-ion diffusion paths and uniform carbon coating can improve the conductivity.

The thin carbon coating on the surfaces of the $LiMnBO_3$ powders could reduce the contact of material with moist air and the corrosion effect by the acidic electrolyte. Therefore, the carbon coating is considered to have positive effect on the cycling performance of the present materials [13,26]. To the best of our survey, it is the first report about the rate performance of m-$LiMnBO_3$/C under constant current charge-discharge mode. In this experiment, the rate performance of Li/m-$LiMnBO_3$/C was tested under different current densities (5 mA g^{-1}, 11 mA g^{-1}, 22 mA g^{-1}). As is shown in Fig. 5b, the initial discharge capacity of m-$LiMnBO_3$/C is 134 mAh g^{-1} at a

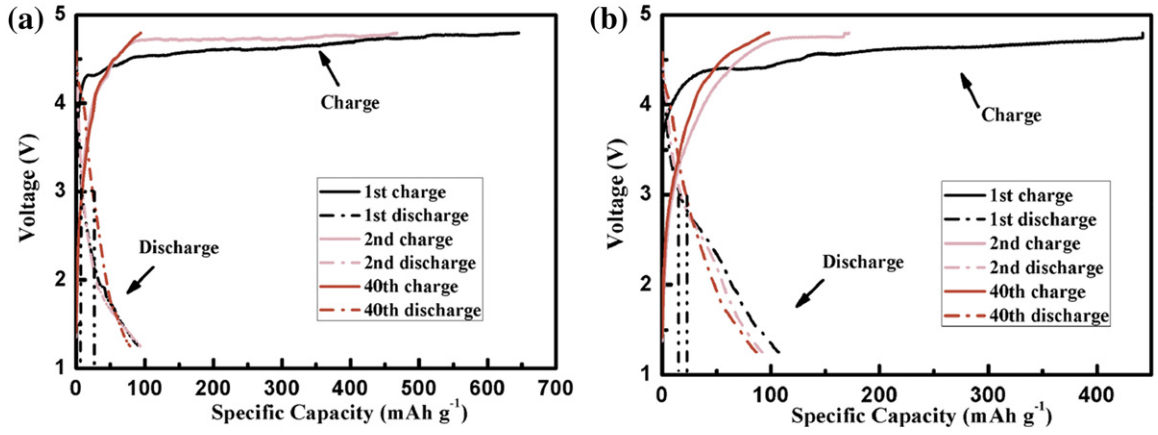

Fig. 4. The charge–discharge curves of $LiMnBO_3$/C electrodes of the 1st, 2nd, and 40th cycle within the voltage range of 1.25–4.80 V vs. Li/Li^+: (a) h-$LiMnBO_3$/C, (b) m-$LiMnBO_3$/C.

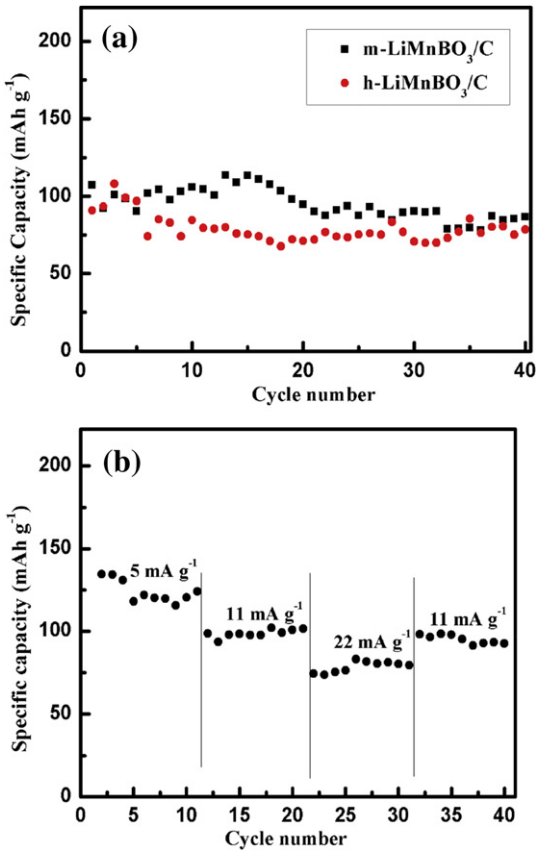

Fig. 5. (a) Specific discharge capacities vs. cycle numbers of h-$LiMnBO_3$/C and m-$LiMnBO_3$/C at 0.05 C in the voltage range: 1.25–4.80 V; (b) Specific discharge capacity of m-$LiMnBO_3$/C at different current densities.

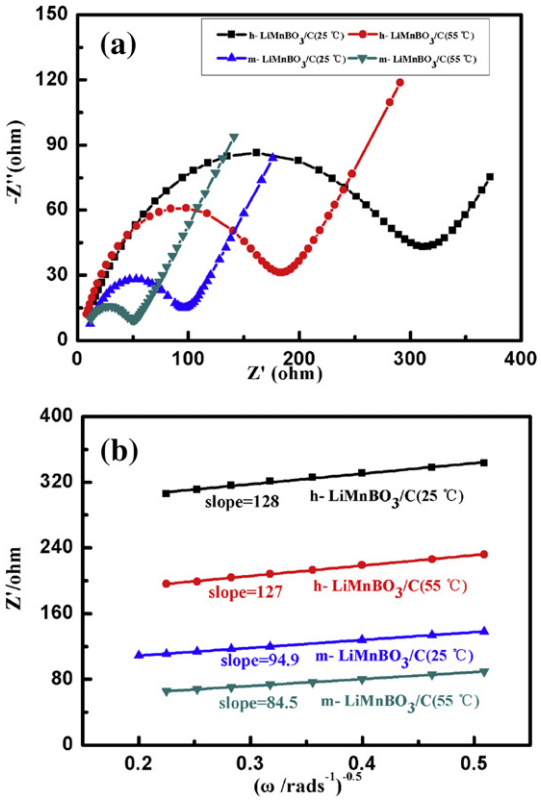

Fig. 6. (a) Nyquist plots of the h-$LiMnBO_3$/C and m-$LiMnBO_3$/C at room temperature and 55 °C before cycle; (b) The plot of Z'axis vs. square root of frequency ($\omega^{-1/2}$).

lower current density (5 mA g^{-1}). Even if the current density is increased to 22 mA g^{-1}, the discharge capacity of 74.4 mAh g^{-1} can still be obtained. When the current density is restored to 11 mA g^{-1}, the discharge capacity retention rate of m-$LiMnBO_3$/C is 99.5% (98.2 mAh g^{-1}). The initial actual discharge capacity of the $LiMnBO_3$ related product is about half of the theoretical one (222 mAh g^{-1}) similar to the $LiCoO_2$ material [27], which might be attributed to their relatively low Li diffusivity, low antisite energy for Li-M site exchange (associated with their interior structure) of the materials, and also the polarization or defect effects aroused by the preparation conditions [9,28,29]. And it is believed that the future optimized preparation conditions and nanosizing could further improve their performances.

The electrochemical impedance spectroscopy (EIS) may be one of the most sensitive tools for the investigation and understanding of differences in the electrode behaviour of h-$LiMnBO_3$/C and m-$LiMnBO_3$/C. Fig. 6a displays the Nyquist plots of the h-$LiMnBO_3$/C and m-$LiMnBO_3$/C at room temperature and at 55 °C at the open circuit voltage (~3.0 V). The electrochemical impedance spectroscopy data were calculated with ZsimpWin software measured according to a typical equivalent circuit depicted in the literature [28]. The ohmic resistance of the electrode (R_1) corresponds to the value of the high frequency intercept of the semicircle with the horizontal axis. The charge transfer resistance (R_{ct}) and constant phase element (CPE) approximately equal to the numerical value of the diameter of the semicircle in the high frequencies on the Z′ axis [28,30]. The value of R_{ct} can be used to evaluate Li ion transfer speed across interfaces between the electrolyte and active electrode materials. It is reported that the cell impedance is mainly determined by R_{ct} from the cathode material [31]. The Warburg impedance (Z_w) associated with lithium ion diffusion in the electrode materials, corresponding to the inclined straight lines in the low frequencies. The parameters of the equivalent circuit and diffusion coefficients of the h-$LiMnBO_3$/C and m-$LiMnBO_3$/C at room temperature and 55 °C are calculated and recorded in Table 2.

The calculated R_{ct} of h-$LiMnBO_3$/C at 55 °C is 172 Ω, which is smaller than that one (349 Ω) at 25 °C; While the R_{ct} of m-$LiMnBO_3$/C at 55 °C is only 48.0 Ω smaller than that one (97.5 Ω) at 25 °C. The above results not only clearly illustrate that R_{ct} value of the $LiMnBO_3$/C material can be dramatically reduced by the elevation of temperature, but also reveal the better performance of m-$LiMnBO_3$/C than h-$LiMnBO_3$/C under the same temperature.

The plot of Z′ axis vs. square root of frequency ($\omega^{-1/2}$) is shown in Fig. 6b. The slopes of the straight lines are used to determine the Warburg diffusion using the equation: $Z_{re} = R_e + R_{ct} + \sigma\omega^{-1/2}$ [32]. The slopes of the straight lines are attributed to the diffusion of the lithium ions into the bulk of the electrode materials, meaning Warburg diffusion (σ). The diffusion coefficients (D) of the h-$LiMnBO_3$/C and m-$LiMnBO_3$/C at room temperature and 55 °C are 3.01×10^{-15}, 3.70×10^{-15}, 4.07×10^{-15}, 6.22×10^{-15} $cm^2\ S^{-1}$, respectively. The values were calculated according to the formula: $D = 0.5\,(RT/AF^2C\sigma)^2$ [30], here R is the gas constant, T is the absolute temperature, A is the surface area of the electrode, F is the Faraday constant, and C is the concentration of lithium ions. The larger diffusion coefficient (m-$LiMnBO_3$/C, at 55 °C) indicates the higher mobility for Li^+ ion diffusion than other button batteries. It is concluded that high temperature can improve the speed of Li^+ ion diffusion. Furthermore, the exchange current densities ($I_0 = RT/nFR_{ct}$) of the h-$LiMnBO_3$/C and m-$LiMnBO_3$/C are higher at 55 °C than that one at 25 °C, respectively. The above results reveals the stronger charge transfer ability of the materials at 55 °C than that at

Table 2
Electrochemical impedance parameters of the h-$LiMnBO_3$/C and m-$LiMnBO_3$/C button battery samples at 25 °C and 55 °C, respectively.

Samples/temperature(°C)	R_1 (Ω)	Q (μF)	R_{ct} (Ω)	σ (Ω cm^2 $S^{-0.5}$)	D (cm^2 S^{-1})	I_0 (mA cm^{-2})
h-$LiMnBO_3$/C (25 °C)	1.73	4.35E-5	349	128	3.01E-15	7.36E-5
h-$LiMnBO_3$/C (55 °C)	2.67	2.59E-5	172	127	3.70E-15	1.65E-4
m-$LiMnBO_3$/C (25 °C)	8.01	2.77E-5	97.5	94.9	4.07E-15	2.63E-4
m-$LiMnBO_3$/C (55 °C)	6.17	2.73E-5	48.0	84.5	6.22E-15	5.89E-4

25 °C, and the better performance of m-$LiMnBO_3$/C than h-$LiMnBO_3$/C [33,34].

4. Conclusions

In this study, m-$LiMnBO_3$/C and h-$LiMnBO_3$/C were selectively synthesized by using $LiOH \cdot H_2O$, $MnCO_3$, H_3BO_3 and ascorbic acid at 500–750 °C via in-situ carbothermal solid state reaction. It is the first time to report the relative long cycle stability (40 cycles) character of h-$LiMnBO_3$/C at the current density of 11 mA g^{-1}. The initial discharge capacity of h-$LiMnBO_3$/C material was 90.7 mAh g^{-1}, and 86.5% of the capacity could be retained after 40 cycles, indicating high cycle stability. It is the first time to show the rate performance of m-$LiMnBO_3$/C. The initial discharge capacity of m-$LiMnBO_3$/C was 107 mAh g^{-1} under the current density of 11 mA g^{-1} (0.05 C), and the capacity of 74.4 mAh g^{-1} could be retained even if the current density was increased to 22 mA g^{-1} (0.1 C). The EIS result indicated that the R_{ct} at 55 °C was smaller than that one at 25 °C, indicating the better electronic conductivity at higher temperature. The convenient synthesis and high performance of the $LiMnBO_3$/C with different phase might enable their wide potential applications as promising cathode materials for lithium-ion rechargeable batteries.

Acknowledgements

This work was supported by the National Nature Science Foundation of China and Academy of Sciences large apparatus United Foundation (Nos. 11179043 and 20971079), and the 973 Project of China (No. 2011CB935901).

Appendix A. Supplementary data

Supplementary data related to this article can be found at http://dx.doi.org/10.1016/j.jpowsour.2013.02.027.

References

[1] L.Q. Xu, S.L. Li, Y.X. Zhang, Y.J. Zhai, Nanoscale 4 (2012) 4900–4915.
[2] L. Chen, Y.M. Zhao, X.N. An, J.M. Liu, Y.Z. Dong, Y.H. Chen, Q. Kuang, J. Alloy Compd. 494 (2010) 415–419.
[3] V. Legagneur, Y. An, A. Mosbah, R. Portal, A. Le Gal La Salle, A. Verbaere, D. Guyomard, Y. Piffard, Solid State Ionics 139 (2001) 37–46.
[4] J.L. Allen, K. Xu, S.S. Zhang, T.R. Jow, Mater. Res. Soc. Symp. P. 730 (2002) 9–14.
[5] S. Afyon, D. Kundu, F. Krumeich, R. Nesper, J. Power Sources 224 (2013) 145–151.
[6] M. Isono, S. Okada, J. Yamaki, J. Power Sources 195 (2010) 593–598.
[7] A. Yamada, N. Iwane, Y. Harada, S. Nishimura, Y. Koyama, I. Tanaka, Adv. Mater. 22 (2010) 3583–3587.
[8] Y.Z. Dong, Y.M. Zhao, Z.D. Shi, X.N. An, P. Fu, L. Chen, Electrochim. Acta 53 (2008) 2339–2345.
[9] D.H. Seo, Y.U. Park, S.W. Kim, I. Park, R.A. Shakoor, K. Kang, Phy. Rev. B 83 (2011) 205127.
[10] O.S. Bondareva, M.A. Simonov, Y.K. Egorov-Tismenko, N.V. Belov, Sov. Phys. Crystallogr. 23 (1978) 269–271.
[11] J.C. Kim, C.J. Moore, B. Kang, G. Hautier, A. Jain, G. Ceder, J. Electrochem Soc. 158 (2011) 309–315.
[12] A. Yamada, N. Iwane, S. Nishimura, Y. Koyama, I. Tanaka, J. Mater. Chem. 21 (2011) 10690–10696.
[13] J. Barker, M.Y. Saidi, J.L. Swoyer, Electrochem. Solid-State Lett. 6 (3) (2003) A53–A55.
[14] K.R. Yang, Z.H. Deng, J.S. Suo, J. Solid State Electrochem 16 (2012) 2805–2813.
[15] J.K. Kim, J.W. Choi, G.S. Chauh an, J.H. Ahn, G.C. Hwang, J.B. Choi, H.J. Ahn, Electrochim. Acta 53 (2008) 8258–8264.
[16] G.D. Li, L.Q. Xu, Q. Hao, M. Wang, Y.T. Qian, RSC Adv. 2 (2012) 284–291.
[17] A.C. Ferrari, J. Robertson, Phys. Rev. B 61 (2000) 14095.
[18] B. David, A. Rodney, J. David, C. Bailin, M. Mark, Nano Lett. 2 (2002) 615–619.
[19] L.X. Yuan, Z.H. Wang, W.X. Zhang, X.L. Hu, J.T. Chen, Y.H. Huang, J.B. Goodenough, Energy Environ. Sci. 4 (2011) 269–284.
[20] Y. Xia, W. Zhang, H. Huang, Y. Gan, Z. Xiao, L. Qian, X. Tao, J. Mater. Chem. 21 (2011) 6498–6501.
[21] W. Liu, Y. Xu, R. Yang, J. Alloys Compd 480 (2009) L1–L4.
[22] R. Dominko, M. Bele, A. Kokalj, M. Gaberscek, J. Jamnik, J. Power Sources 174 (2007) 457–461.
[23] V. Aravindan, K. Karthikeyan, S. Ravi, S. Amaresh, W.S. Kim, Y.S. Lee, J. Mater. Chem. 20 (2010) 7340–7343.
[24] J. Liu, H.Y. Xu, X.L. Jiang, J. Yang, Y.T. Qian, J. Power Sources 231 (2013) 39–43.
[25] S.H. Bo, F. Wang, Y. Janssen, D.L. Zeng, K.W. Nam, W.Q. Xu, L.S. Du, J. Graetz, X.Q. Yang, Y.M. Zhu, J.B. Parise, C.P. Grey, P.G. Khalifah, J. Mater. Chem. 22 (2012) 8799–8809.
[26] H.S. Kim, K. Kim, S.I. Moon, I.J. Kim, H.B. Gu, J. Solid State Electrochem. 12 (2008) 867–872.
[27] X. Zuo, C. Fan, X. Xiao, J. Liu, J. Nan, J. Power Sources 219 (2012) 94–99.
[28] V. Aravindan, K. Karthikeyan, S. Amaresh, Y.S. Lee, Bull. Korean Chem. Soc. 31 (2010) 1506–1509.
[29] Y. Janssen, D.S. Middlemiss, S.H. Bo, C.P. Grey, P.G. Khalifah, J. Am. Chem. Soc. 134 (30) (2012) 12516–12527.
[30] A.Y. Shenouda, H.K. Liu, J. Alloys Compd 477 (2009) 498–503.
[31] C.H. Chen, J. Liu, K. Amine, J. Power Sources 96 (2001) 321–328.
[32] Y. Cui, X.L. Zhao, R.S. Guo, Electrochim. Acta 55 (2010) 922–926.
[33] B. Jin, E.M. Jin, K. Park, H. Gu, Electrochem. Commun. 10 (2008) 1537–1540.
[34] A.Y. Shenouda, H.K. Liu, J. Electrochem. Soc. 157 (2010) 1183–1187.

Glossary

m-$LiMnBO_3$: monoclinic $LiMnBO_3$
h-$LiMnBO_3$: hexagonal $LiMnBO_3$
m-$LiMnBO_3$/C: carbon-coated monoclinic $LiMnBO_3$
h-$LiMnBO_3$/C: carbon-coated hexagonal $LiMnBO_3$
EIS: electrochemical impedance spectroscopy
XRD: X-ray diffraction
TEM: transmission electron microscopy
FESEM: field emission scanning electron microscope
HRTEM: high-resolution transmission electron microscopy
PVDF: poly(vinylidene fluoride)
NMP: n-methylpyrrolidone
EC: ethylene carbonate
DMC: dimethyl carbonate
DEC: diethyl carbonate
R_{ct}: charge transfer resistance
Z_w: Warburg impedance
D: diffusion coefficients
CPE: constant phase element